Electronic Supplementary Information

Characterizations

Hitachi S-4800 scanning electron microscope (SEM) was used to characterize the morphology. JEOL-2100F transmission electron microscopy (TEM) was employed to investigate the structure and composition of catalysts. X-ray diffraction (XRD) pattern was conducted on a PANalytical X'Pert Powder with Cu Kα radiation X-ray source (λ = 0.154056 nm). X-ray photoelectron spectra (XPS) spectrum was carried out by ESCALAB MK II spectrometer (VG Scientific, UK) with Al Kα X-ray excitation.

Electrochemical investigations

The electrochemical measurements were carried out on a CHI 852D electrochemical analyzer with a three-electrodes cell which includes a Pt wire, a Ag/AgCl (3 M KCl), and a rotating disk electrode (RDE) as a counter electrode, reference electrode, and working electrode, respectively. The working electrode was modified with different catalysts (2 μg of catalyst), and then coated with 3 μL of Nafion (0.5%), left to fully dry before the measurements. The linear sweep voltammograms (LSVs) are performed on an RRDE-3A rotation system (ALS Co. Ltd, Japan) in an O_2-saturated 0.1 M $HClO_4$ at a sweep rate of 5 mV s^{-1} with a rotation speed of 1600 rpm. The electron transfer number (n) is calculated by the Koutecky-Levich equation as follow:

$$\frac{1}{j} = \frac{1}{j_k} + \frac{1}{j_d}$$

$$j_d = 0.2nFD^{2/3}v^{-1/6}\omega^{1/2}\,C_{O2}$$

Where, j, j_k, and j_d are the measured, kinetic, and diffusion currents, respectively. F is the Faraday's constant (96485 C mol^{-1}). D is the diffusion coefficient of O_2 (1.93×10^{-5} cm^2 s^{-1}), v is the kinetic viscosity (1.13×10^{-2} cm^2 s^{-1}), ω is the rotation speed of electrode (rpm), and C_{O2} is the bulk concentration of O_2 dissolved in 0.1 M $HClO_4$ (1.22×10^{-3} mol L^{-1}).

The electrochemical active surface areas (ECSAs) are calculated using the following equation:

$$\text{ECSA} = Q / m \times 210$$

Where m is the Pt loading on the electrode surface, 210 μC cm^{-2} is the charge required for monolayer adsorption of hydrogen on the Pt surface, and Q is the charge in the Hupd adsorption/desorption area obtained after the double layer correction.

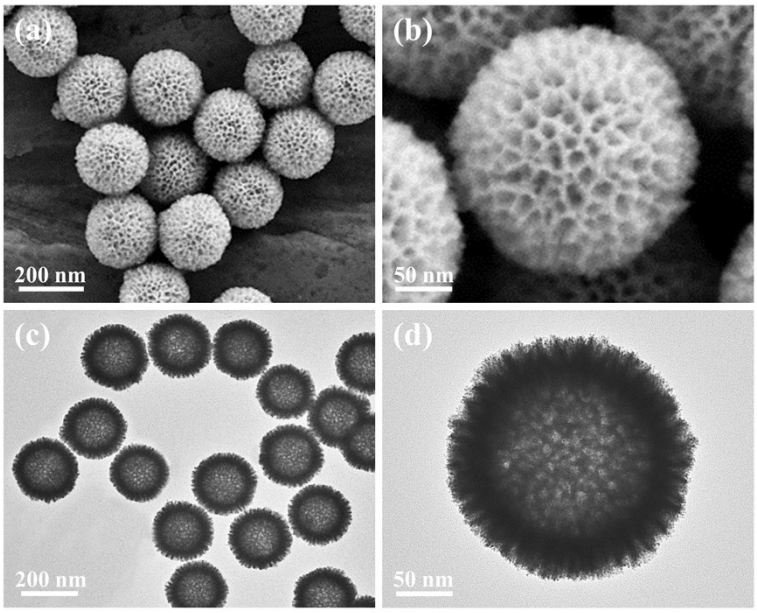

Fig. S1 (a, b) SEM images and (c, d) TEM images of the PtPd mNCs.

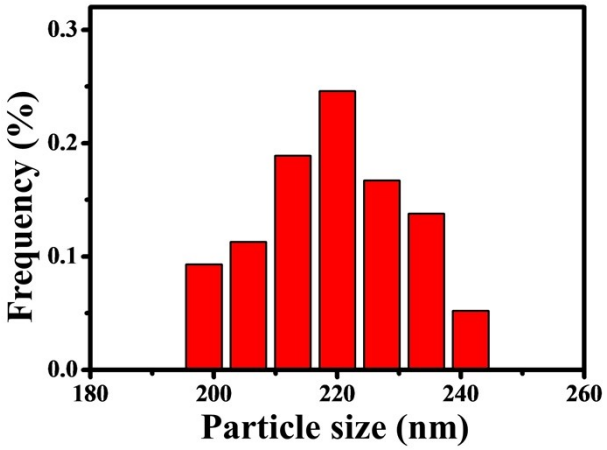

Fig. S2 The size distribution histogram of the PtPdSP mNCs.

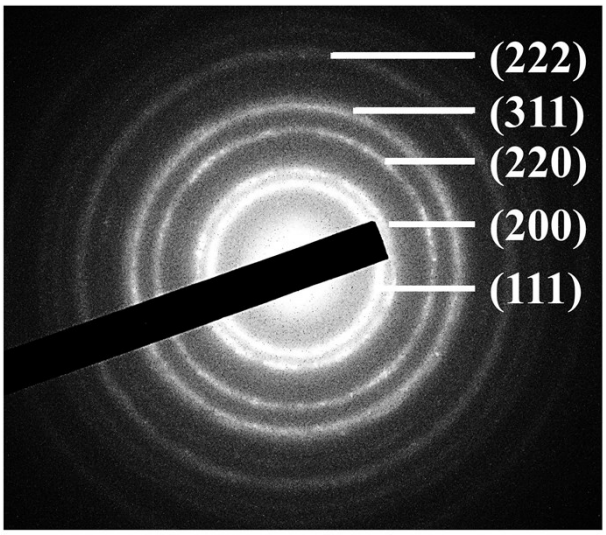

Fig. S3 SAED pattern of the PtPdSP mNCs.

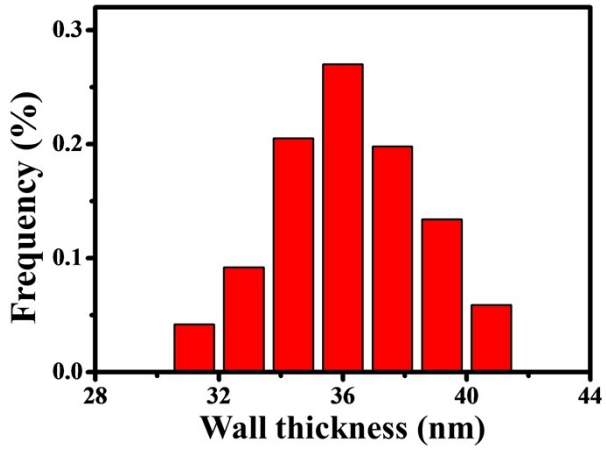

Fig. S4 The wall thickness distribution histogram of the PtPdSP mNCs.

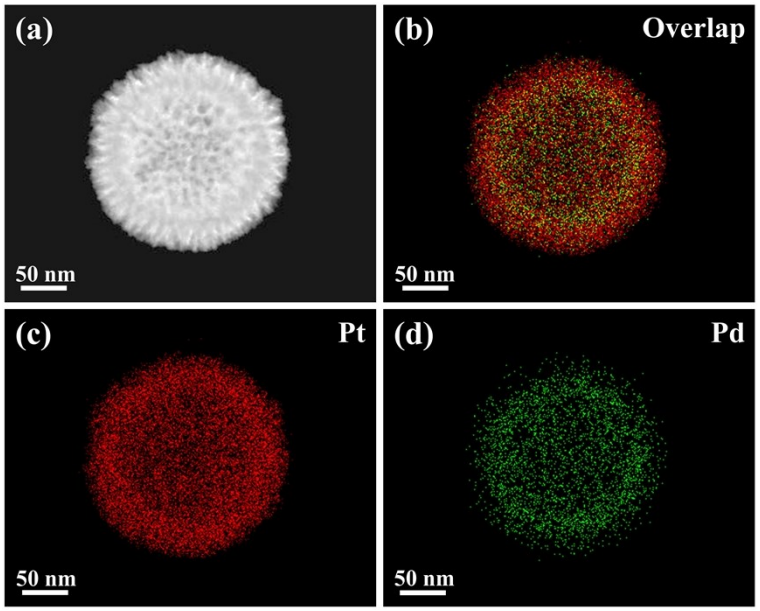

Fig. S5 (a) HAADF-STEM image of a PtPd mNC. (b-d) Elemental mapping images of the PtPd mNC.

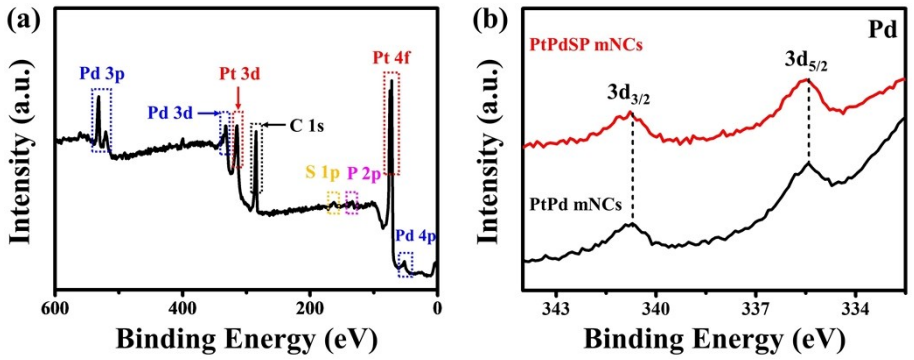

Fig. S6 (a) XPS spectrum for the PtPdSP mNCs. (b) XPS spectra of Pd 3d for PtPdSP mNCs and PtPd mNCs.

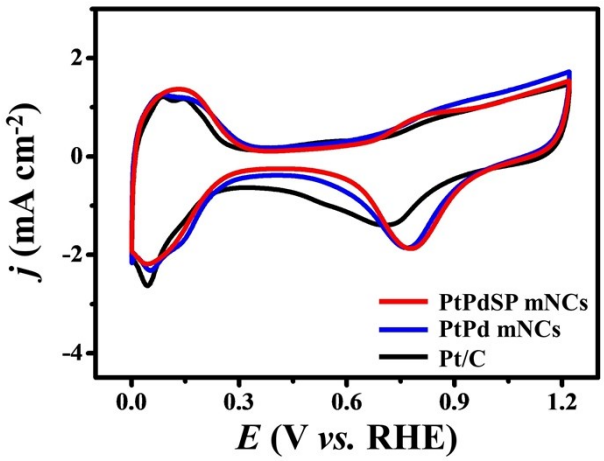

Fig. S7 CV curves of the three catalysts in an N_2-saturated 0.1 M $HClO_4$ solution.

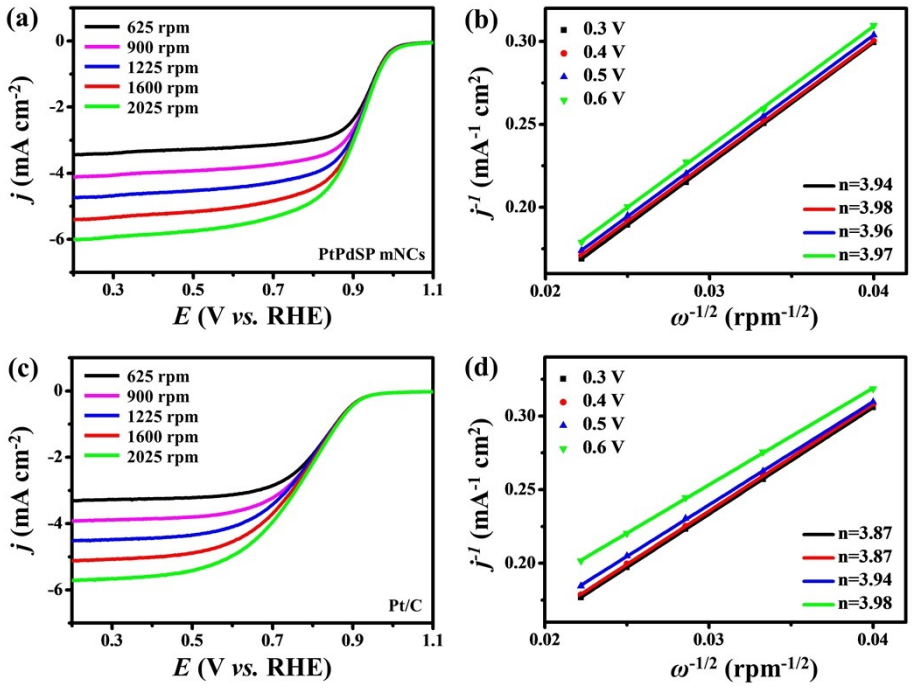

Fig. S8 (a) ORR polarization curves with different RDE rotation rates, and (b) the electron transfer numbers at different potentials of the PtPdSP mNCs. (c) ORR polarization curves with different RDE rotation rates, and (d) the electron transfer numbers at different potentials of the Pt/C.

Table S1 The comparisons of the ORR performance of the PtPdSP mNCs with some recently reported Pt-based catalysts.

Catalyst	E_{onset} (V *vs.* RHE)	$E_{1/2}$ (V *vs.* RHE)	Ref.
PtPdSP mNCs	**1.03**	**0.91**	**This work**
PtAu nanoparticles	0.98	0.83	1
Porous PtAg hollow chain-like networks	0.933	0.857	2
PtCo nanomyriapods	0.92	0.82	3
PtPd networks	0.89	/	4
Nanoporous Pt	0.85	/	5
Pt nanoparticles	0.85	/	6
Dodecahedral CuPt nanoframes	/	0.87	7
MCS Au@PtNi NPs	/	0.838	8

Table S2 The comparisons of the specific activity (SA) and mass activity (MA) of the PtPdSP mNCs with some recently reported Pt-based catalysts.

Catalyst	SA (mA cm^{-2})	MA (A mg^{-1}_{Pt})	Ref.
PtPdSP mNCs	**1.10**	**0.56**	**This work**
PtCu/CNT	0.45941	0.30525	9
Pt_3Ni_3MoN/C	0.1554	0.53941	10
Pt/Pd/C	1.172	0.434	11
NP–$Pt_{75}Pd_{25}$	0.39	0.25	12
Au–Pd–Pt NFs/rGO	0.479	0.212	13
Pt–Pd–Ag/C nanoflowers	0.526	0.206	14
np-PtCuTi catalyst	0.84	0.256	15
$Pt_5Cu_{76}Co_{11}Ni_8$ NTs	0.18	0.19	16

References

1 W. Wu, Z. Tang, K. Wang, Z. Liu, L. Li and S. Chen, *Electrochim. Acta,* 2018, **260**, 168−176.

2 A. Wang, L. Liu, X. Lin, J. Yuan and J. Feng, *Electrochim. Acta,* 2017, **245**, 883−892.

3 L. Jiang, X. Huang, A. Wang, X. Li, J. Yuan and J. Feng, *J. Mater. Chem. A.,* 2017, **5**, 10554−10560.

4 Y. Shi, L. Mei, A. Wang, T. Yuan, S. Chen and J. Feng, *J. Colloid Interf. Sci.,* 2017, **504**, 363−370.

5 B. Geboes, J. Ustarroz, K. Sentosun, H. Vanrompay, A. Hubin, S. Bals and T. Breugelmans, *ACS Catal.,* 2016, **6**, 5856−5864.

6 R. Devivaraprasad, R. Ramesh, N. Naresh, T. Kar, R. Singh and M. Neergat, *Langmuir,* 2014, **30**, 8995–9006.

7 L. Lyu, Y. Kao, D. Cullen, B. Sneed, Y. Chuang and C. Kuo, *Chem. Mater.,* 2017, **29**, 5681−5692.

8 Q. Shi, C. Zhu, S. Fu, D. Du and Y. Lin, *ACS Appl. Mater. Interfaces,* 2016, **8**, 4739−4744.

9 H. El-Deeb and M. Bron, *Electrochim. Acta,* 2015, **164**, 315−322.

10 L. Luo, H. S. Abbo, S. J.J. Titinchi, P. Tsiakaras and S. Yin, *Int. J. Hydrogen energy,* 2019, **44**, 6582−6591.

11 N. Aoki, H. Inoue, T. Okawa, Y. Ikehata, A. Shirai, H. Daimon, T. Doi, Y. Orikasa, Y. Uchimoto, H. Jinnai, S. Inamoto, Y. Otsuka and M. Inaba, Electrocatalysis, 2018, 9, 125−138.

12 H. Duan and C. Xu, *Electrochim. Acta,* 2015, **152**, 417−424.

13 L. Huang, Y. Han and S. Dong, *Chem. Commun.,* 2016, **52**, 8659−8662.

14 A. Chalgin, F. Shi, F. Li, Q. Xiang, W. Chen, C. Song, P. Tao, W. Shang, T. Deng and J. Wu, *CrystEngComm,* 2017, **19**, 6964−6971.

15 Y. Wang, K. Yin, J. Zhang, C. Si, X. Chen, L. Lv, W. Ma, H. Gao and Z. Zhang, *J. Mater. Chem. A,* 2016, **4**, 14657−14668.

16 L. Liu and E. Pippel, *Angew. Chem., Int. Ed.,* 2011, **50**, 2729−2733.